Searching for Dark Matter with Precision Pulsar Timing

Adapted for the Merton U3A

John M. LoSecco

Physics and Astronomy Department, University of Notre Dame, Notre Dame, IN 46556-5670, USA

October 2024

Abstract

This talk describes searches for evidence of dark matter concentrations along the path of radio pulses in the PPTA2 survey data release. Radio pulse travel times are influenced via gravitational fields along the path from the source to the observer. Transient time delays in transit are a useful measure of the matter distribution along the path. Many pulsars have very well understood timing solutions with predicable arrival times and can be used to sample the mass induced variation. Changes in the source, observer and dark matter positions produce changes in arrival times which can be significant for precision pulsar times. Twelve candidates are reported from this search.

Doppler Shift

When the emiter and reciever of a wave phenomena have relative velocity toward or away from each other the transmitted and recieved wave will have different frequencies.When the emiter and reciever are approaching each other the recieved frequency will be higher than the transmitted one. When they are moving appart it will be lower.

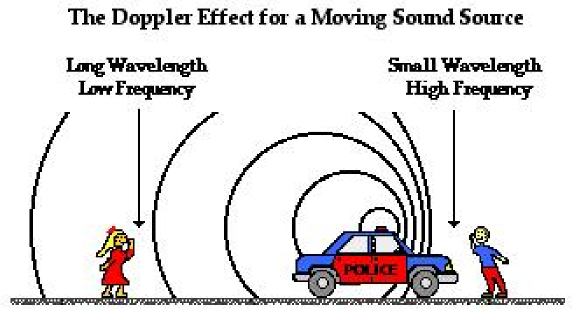

$$\lambda_{obs} = \lambda_{src}(1 + \frac{v}{c})\sqrt{\frac{1}{1-\frac{v^2}{c^2}}} \approx \lambda_{src}(1 + \frac{v}{c})$$

The Equivalence Principle

A gravitational “force” is equivalent to an accelerating reference frame.

In free fall you have no effects of gravitation.

All objects fall at the same speed regardless of their mass.

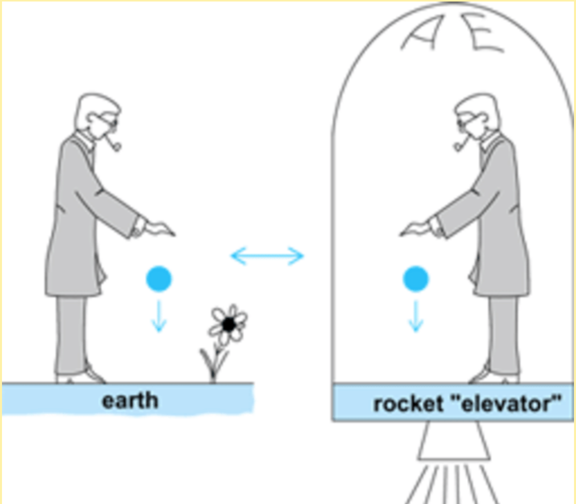

Gravitational Time Dilation

It follows from the equivalence principle that clocks run more slowly in a gravitational field.

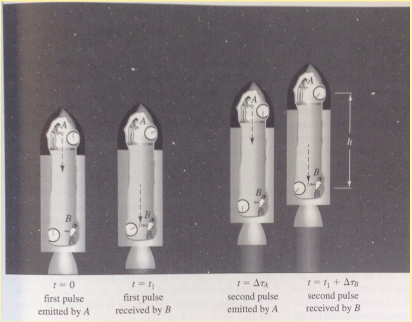

A rocket moving with constant acceleration upward is equivalent to a gravitational field pointing down. A pulse sent up from the bottom arrives at the top to a receiver which is moving away at a faster speed. A pulse sent down from the top arrives at the bottom to a receiver which is moving toward it at a faster speed.

Gravitational Time Delay II

The pulses are Doppler shifted. The lower clock is slower than the top one and the top one is faster than the bottom one. Pulses sent up to the top at equal time intervals arrive at equal time intervals which are larger. Similarly pulses sent down to the bottom at equal time intervals arrive at equal time intervals which are shorter.
The faster speed when the pulses are received is because the rocket is accelerating. During the time it takes for the pulse to move from one end to the other he speed of the rocket has increased.
Observers higher in the gravitational field see the clocks lower down running more slowly since pulses from below arrive further apart than pulses from the local clock.

First Observations of the Delay -1967

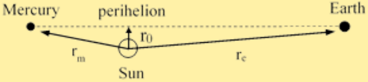

The cumulative effect of being in a gravitational field is longer time intervals. This was calculated in the 1960's by Shapiro who observed the time delay due to the sun's gravitational field on radar pulses being bounced off of Mercury as Mercury went behind the sun.

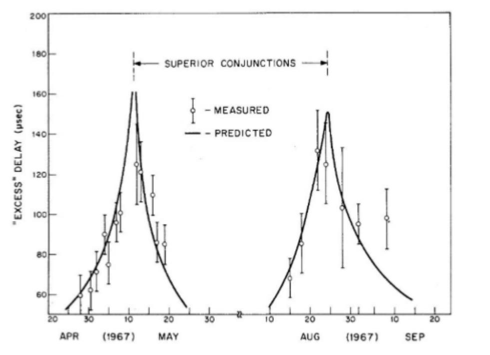

The Time Delay – Dark Matter

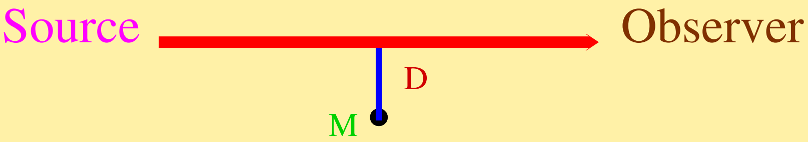

The impact parameter D and the gravitating mass $\mathcal{M}$ are shown.

$$\Delta T = -\frac{2G\mathcal{M}}{c^3}\ln(1 - \hat{R}\cdot\hat{s}) \qquad (1)$$

$\frac{2G\mathcal{M}}{c^3}$ is the Schwarzschild radius divided by the speed of light and $\hat{R}\cdot\hat{s}$ is the cosine of the angle, as viewed from the observer, between the source of the pulse and the source of the gravitational field created by mass $\mathcal{M}$. For reference $\frac{2G\mathcal{M}_{Sun}}{c^3}$ is 9.85 microseconds.

Time Delay Illustration

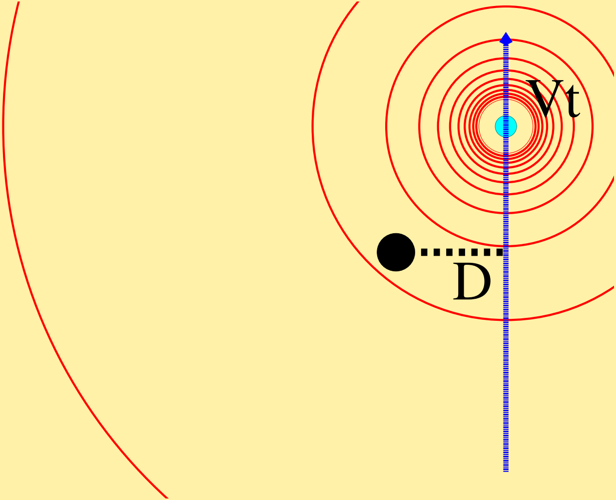

As the dark matter (cyan dot) moves, the pulsar beam (black dot) goes through regions of decreasing then increasing gravitational potential. Time runs more slowly the deeper the potential. The rings express uniformly spaced equipotential surfaces

Time Dependence

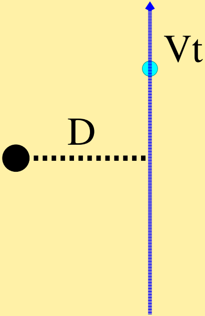

The time dependent geometry of the pulsar - dark matter cosine as viewed by the observer is on the left. The Z axis goes from the observer to the pulsar (dot on the left). The point of closest approach is a distance D along the X axis. The Y coordinate is upward along the projected speed of the dark matter. The displacement along Y is taken as Vt. The dark matter is in the plane at (D,Vt).

$$\Delta T = -M \ln\left(1 - \frac{1}{\sqrt{1+(v(t-t_0))^2+d^2}}\right)$$

$M = \frac{2G\mathcal{M}}{c^3}$, $v = V/Z$ and $d = D/Z$

The Data

The PPTA2 release includes 65 millisecond pulsars and their fits. This data was processed with Tempo2 to provide residuals, the deviation of the pulse arrival time from the time estimated by the model. These residuals hold information about potential encounters with massive bodies on route to the detector. The data includes observations from 7 radio telescopes, Effelsberg, Lovell, Nançay, Westerbork, Green Bank, Arecibo and Parkes.
The pulsar data samples span varying time intervals from 231 to 10753 days and have from 116 to 17487 fitted pulses. A total of 210148 pulse residuals over a total time period of 255327 MJD are provided in the release.

Summary of the Data – Event Found

Pulsar	Sample Length (MJD)	Sample Size	Candidates
J0034-0534	4935.41	276	1
J0613-0200	5863.88	9322	2
J1024-0719	6647.34	5865	3
J1640+2224	6301.78	3097	1
J1643-1224	7356.24	8136	2
J1713+0747	8201.93	17487	1
J1857+0943	10344.48	5004	1
J1909-3744	3951.20	11483	1

Sample Fit

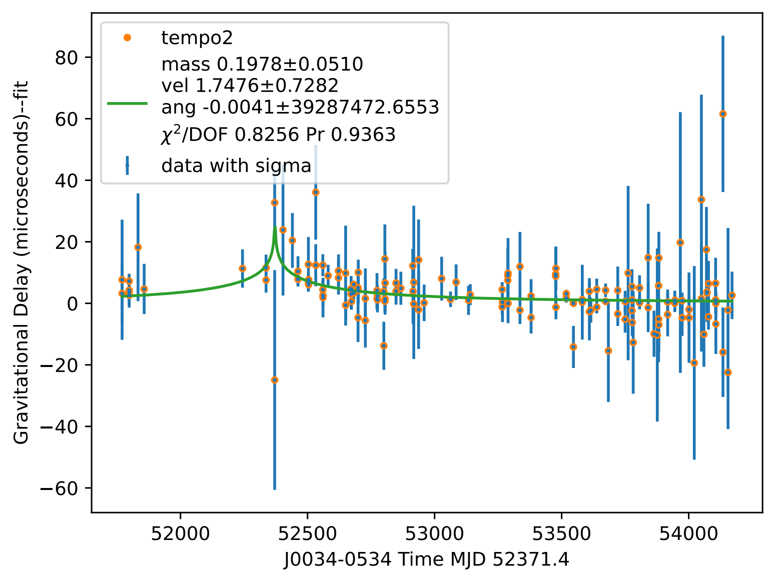

A fit to pulsar J0034-0534 showing a significant delay at 52371.4 MJD

Method

The method used has two parts. The first part searches for signal delay candidates over a limited portion of the recorded data. Once found a local fit is done on that candidate to recover the fit parameters. Based on gravitational lensing results the encounters are expected to occur over a period of weeks or months. The data sample span periods from less than a year to almost 30 years. The method adopted is to fit *overlapping* regions of about 120 consecutive residuals, less if necessary. A modest event candidate is refit with the candidate time at the center of the interval. When possible the width of the refit is when the deviation has dropped to 10% of the preliminary peak height.

To proceed from the search fit to the centered fit the search result must have a log likelihood ratio test at the 95% level. The fit itself should have an Anderson-Darling test for Gaussian residuals at the 95% level and the absolute value of the fitted mass, $|M|$ must be at least 3 time its σ.

Results

2084 candidates pass the search criteria to be re-centered and refit. After the refit 108 of these have $|M|/\sigma_M > 3$. 16 of these have a fit with a χ^2/DOF probability > 0.1. Four of these candidates are duplicates with similar but not identical data, leaving 12 independent signal candidates. 8 pulsars are represented.

Table of Results

Pulsar	Sample	Duration	Count	RMS	Prob	$\mathcal{M} \pm \sigma_{\mathcal{M}}$	$\mathcal{M}/\sigma_{\mathcal{M}}$
J0613-0200	19	236.8	457	3.551	0.9995	0.01644 $\pm$ 0.004938	3.329
J1024-0719	29	111.7	414	10.54	0.9139	-0.4137 $\pm$ 0.07403	-5.588
J0034-0534	0	2011.4	109	9.095	0.8481	0.168 $\pm$ 0.0389	4.314
J1024-0719	75	94.7	446	7.891	0.6924	0.3192 $\pm$ 0.1049	3.042
J1713+0747	211	53.3	452	2.111	0.6369	0.03642 $\pm$ 0.009973	3.652
J1640+2224	3	84.1	153	4.339	0.6173	0.06589 $\pm$ 0.01322	4.984
J1857+0943	46	127.4	403	2.747	0.4474	0.05748 $\pm$ 0.009663	5.948
J1909-3744	175	54.2	476	1.273	0.2458	0.01408 $\pm$ 0.003733	3.772
J1643-1224	17	230.7	399	3.563	0.1902	0.4636 $\pm$ 0.09352	4.957
J1024-0719	39	123.7	442	10.72	0.1343	-0.2983 $\pm$ 0.07129	-4.184
J0613-0200	72	70	436	2.661	0.1122	0.03849 $\pm$ 0.01255	3.068
J1643-1224	1	1765.6	103	10.78	0.1056	-2.206 $\pm$ 0.4336	-5.087

Masses have been converted to solar masses.

Conclusions

- This is a promising method for observing gravitational inhomogeneities in the galaxy.
- There are clearly selection biases, such as the directions to available pulsars, gaps in the record and sources of noise.
- Possible improvements could be found in fluctuations in the radio flux and distortion of the “image“ at the same time as the delays. These are also signals of a gravitational encounter.
- Identification of such time fluctuations might help the primary goal for this data sample, searching for low frequency gravitational waves, by removing a source of noise.

Candidate Event Plots

Ordered by decreasing χ^2/DOF probability

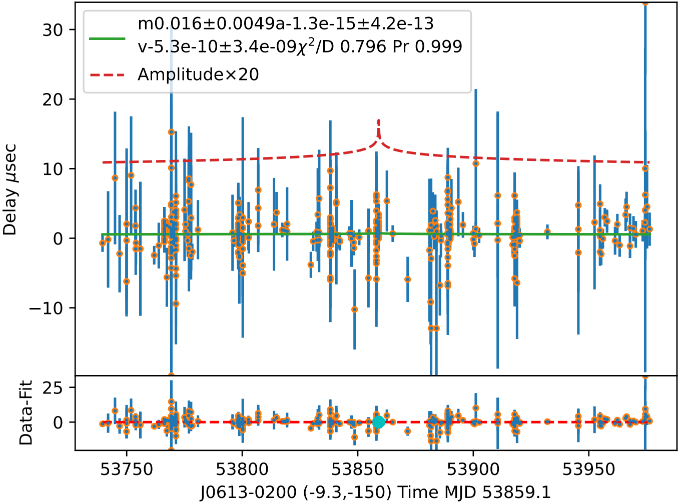

m0.016±0.0049a-1.3e-15±4.2e-13
v-5.3e-10±3.4e-09χ^2/D 0.796 Pr 0.999
Amplitude×20
Delay μsec
Data-Fit
30
20
10
0
−10
25
0
53750
53800
53850
53900
53950
J0613-0200 (-9.3,-150) Time MJD 53859.1

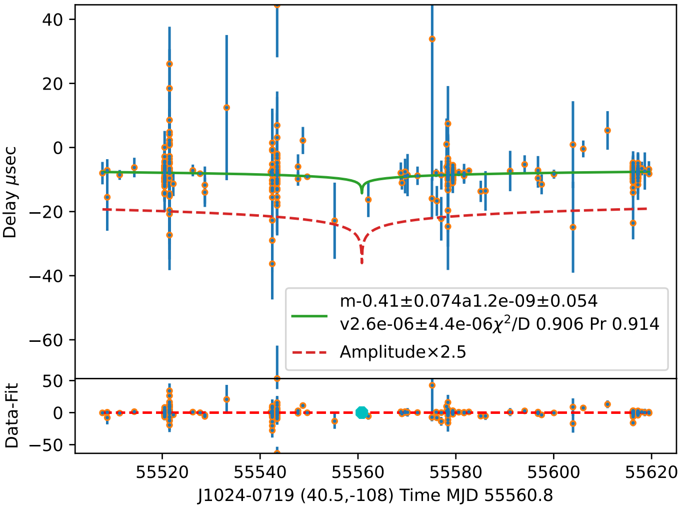

m-0.41±0.074a1.2e-09±0.054
v2.6e-06±4.4e-06χ2/D 0.906 Pr 0.914
Amplitude×2.5
Delay μsec
Data-Fit
J1024-0719 (40.5,-108) Time MJD 55560.8

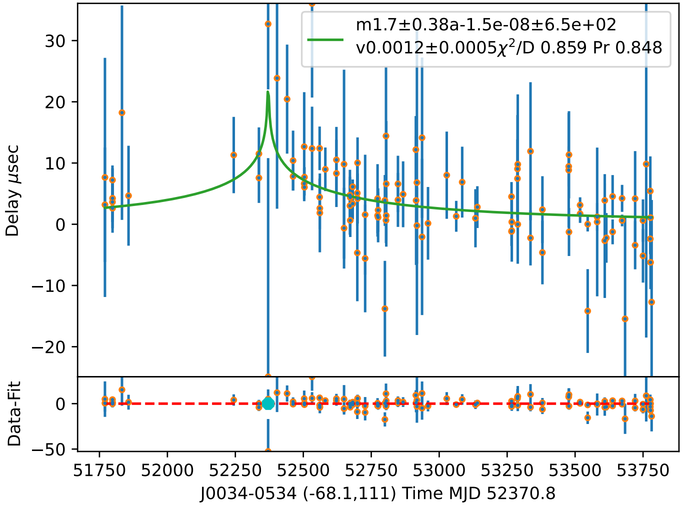

The mass printed on the plot is in microseconds. It is 0.168 ± 0.039 solar masses.

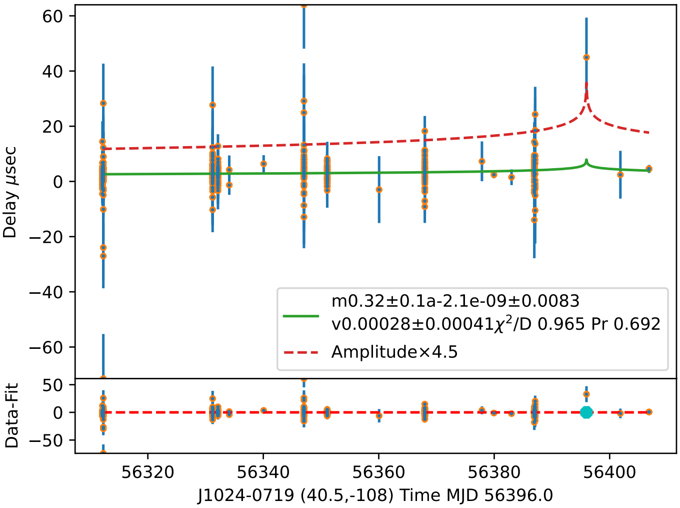
60
40
20
0
−20
−40
−60
Delay μsec
m0.32±0.1a-2.1e-09±0.0083
v0.00028±0.00041χ^2/D 0.965 Pr 0.692
Amplitude×4.5
50
0
−50
Data-Fit
56320
56340
56360
56380
56400
J1024-0719 (40.5,-108) Time MJD 56396.0

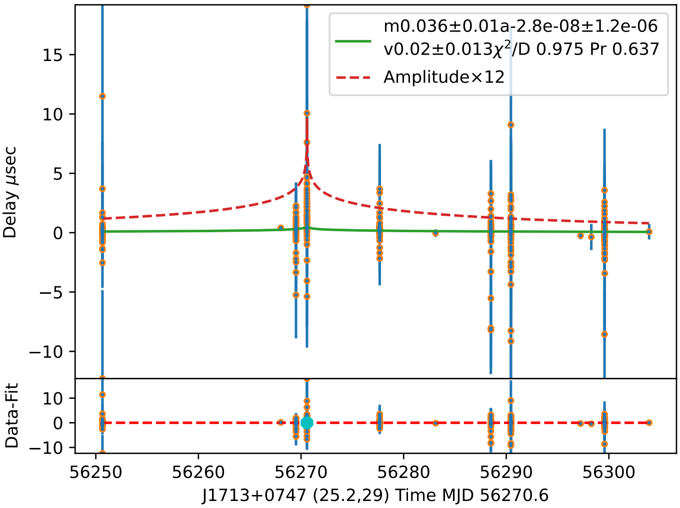
m0.036±0.01a-2.8e-08±1.2e-06
v0.02±0.013χ²/D 0.975 Pr 0.637
Amplitude×12
Delay μsec
Data-Fit
15
10
5
0
−5
−10
56250
56260
56270
56280
56290
56300
J1713+0747 (25.2,29) Time MJD 56270.6

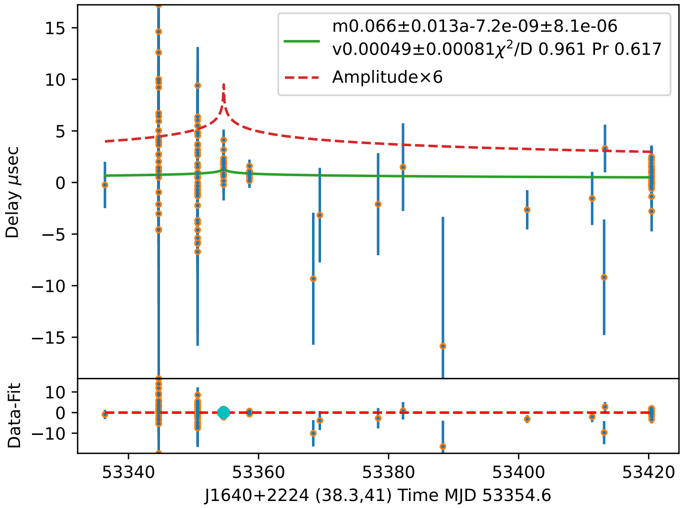

m0.066±0.013a-7.2e-09±8.1e-06
v0.00049±0.00081χ^2/D 0.961 Pr 0.617
Amplitude×6
Delay μsec
Data-Fit
15
10
5
0
−5
−10
−15
53340
53360
53380
53400
53420
J1640+2224 (38.3,41) Time MJD 53354.6

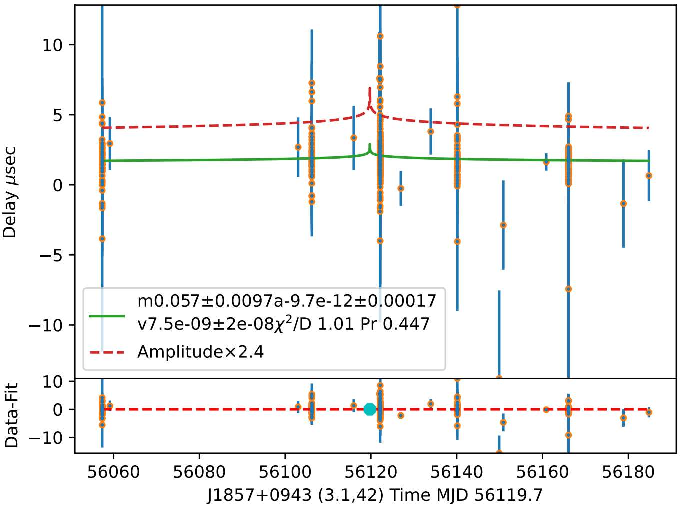

10
5
0
−5
−10
Delay μsec
m0.057±0.0097a-9.7e-12±0.00017
v7.5e-09±2e-08χ2/D 1.01 Pr 0.447
Amplitude×2.4
10
0
−10
Data-Fit
56060
56080
56100
56120
56140
56160
56180
J1857+0943 (3.1,42) Time MJD 56119.7

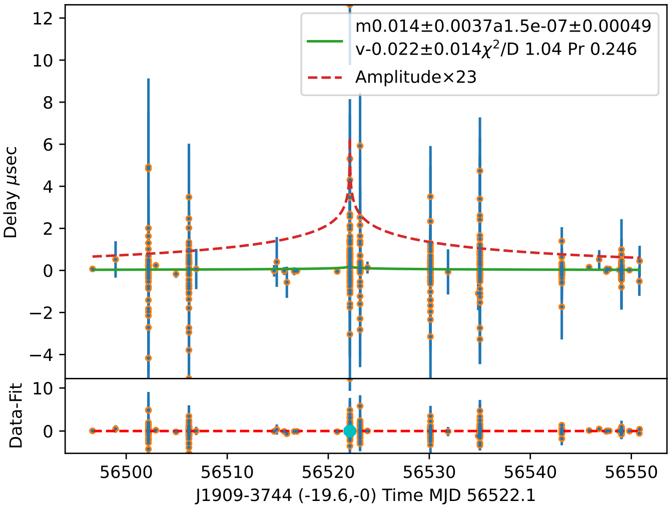

m0.014±0.0037a1.5e-07±0.00049
v-0.022±0.014χ2/D 1.04 Pr 0.246
Amplitude×23
Delay μsec
Data-Fit
J1909-3744 (-19.6,-0) Time MJD 56522.1

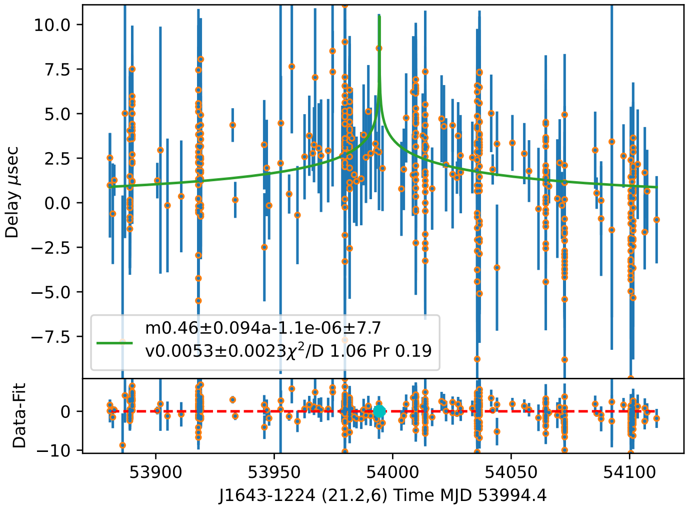

10.0
7.5
5.0
2.5
0.0
−2.5
−5.0
−7.5
Delay μsec
m0.46±0.094a-1.1e-06±7.7
v0.0053±0.0023χ²/D 1.06 Pr 0.19
Data-Fit
0
−10
53900
53950
54000
54050
54100
J1643-1224 (21.2,6) Time MJD 53994.4

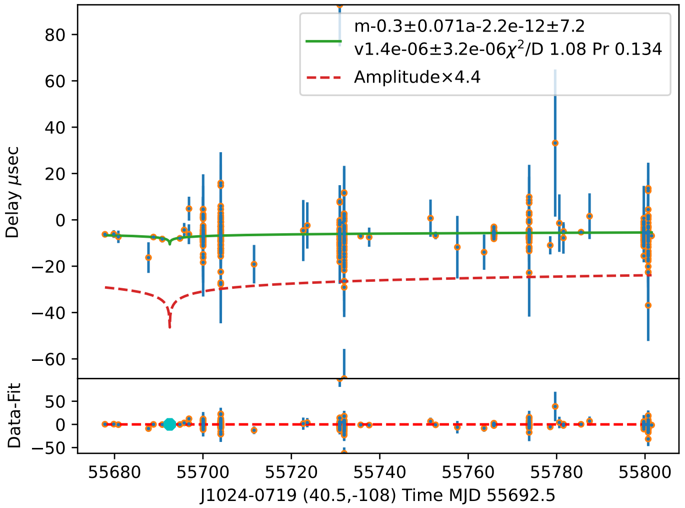
m-0.3±0.071a-2.2e-12±7.2
v1.4e-06±3.2e-06χ²/D 1.08 Pr 0.134
Amplitude×4.4
Delay μsec
Data-Fit
J1024-0719 (40.5,-108) Time MJD 55692.5

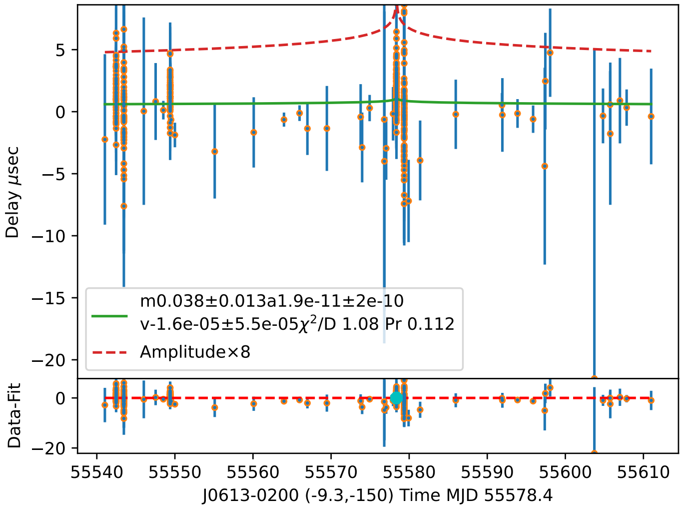

Delay μsec
Data-Fit
m0.038±0.013a1.9e-11±2e-10
v-1.6e-05±5.5e-05χ^2/D 1.08 Pr 0.112
Amplitude×8
5
0
−5
−10
−15
−20
0
−20
55540
55550
55560
55570
55580
55590
55600
55610
J0613-0200 (-9.3,-150) Time MJD 55578.4

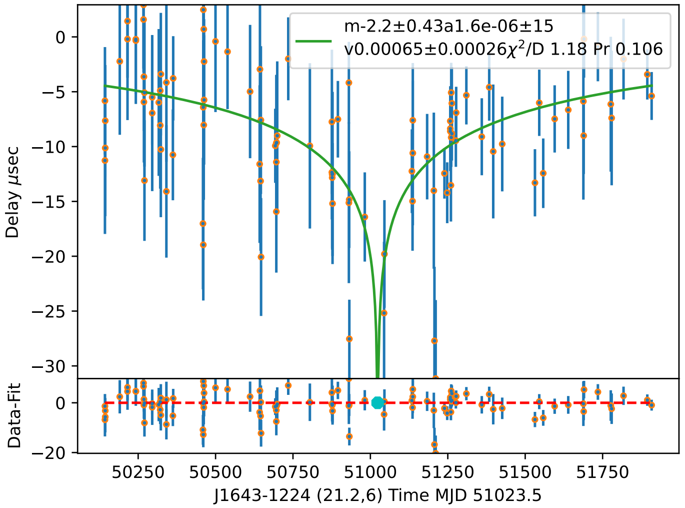

m-2.2±0.43a1.6e-06±15
v0.00065±0.00026χ²/D 1.18 Pr 0.106
Delay μsec
0
−5
−10
−15
−20
−25
−30
Data-Fit
0
−20
50250
50500
50750
51000
51250
51500
51750
J1643-1224 (21.2,6) Time MJD 51023.5

Events that do not pass cuts

A biased selection of convincing fits

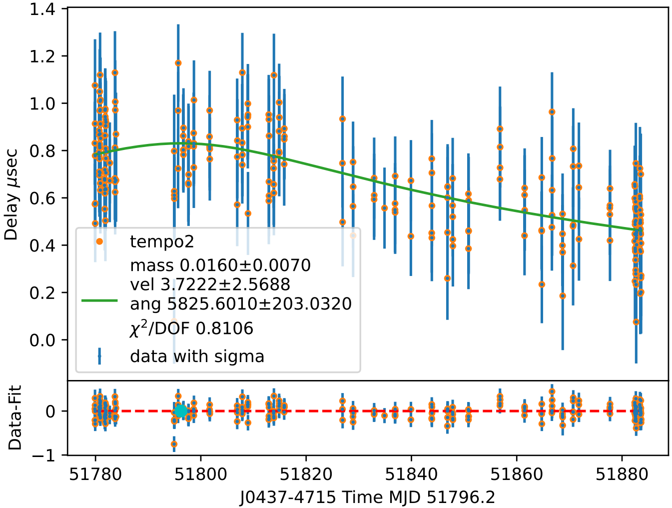

1.4
1.2
1.0
0.8
0.6
0.4
0.2
0.0
Delay μsec
tempo2
mass 0.0160±0.0070
vel 3.7222±2.5688
ang 5825.6010±203.0320
χ2/DOF 0.8106
data with sigma
Data-Fit
0
−1
51780
51800
51820
51840
51860
51880
J0437-4715 Time MJD 51796.2

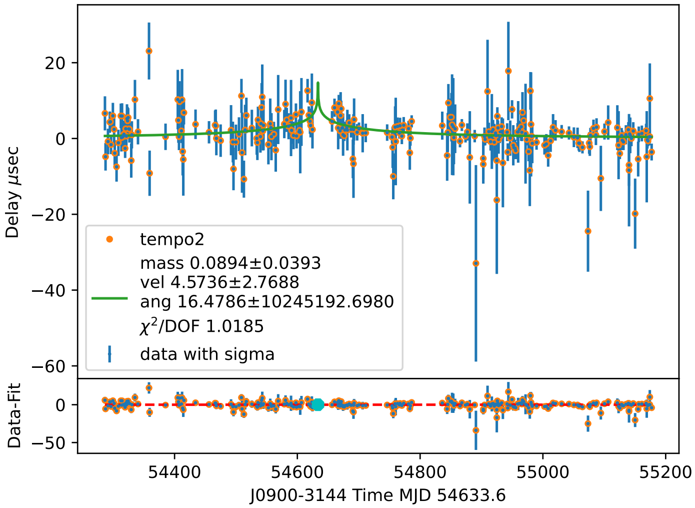

20
0
−20
−40
−60
Delay μsec
tempo2
mass 0.0894±0.0393
vel 4.5736±2.7688
ang 16.4786±10245192.6980
χ²/DOF 1.0185
data with sigma
Data-Fit
0
−50
54400
54600
54800
55000
55200
J0900-3144 Time MJD 54633.6

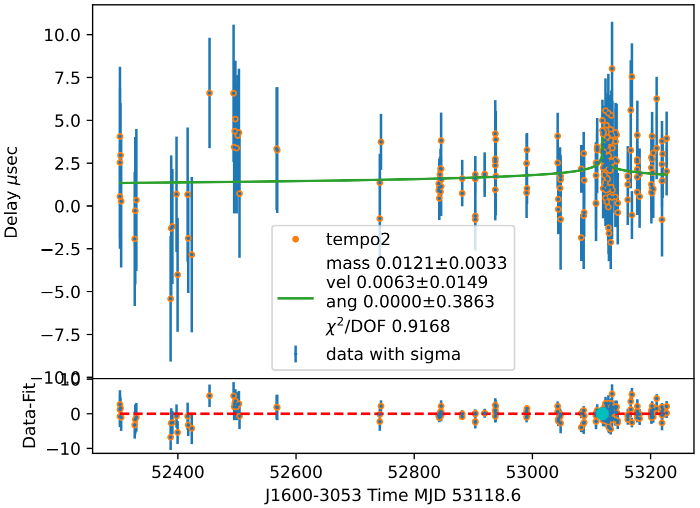

10.0
7.5
5.0
2.5
0.0
−2.5
−5.0
−7.5
−10.0
Delay μsec
tempo2
mass 0.0121±0.0033
vel 0.0063±0.0149
ang 0.0000±0.3863
χ^2/DOF 0.9168
data with sigma
10
0
−10
Data-Fit
52400
52600
52800
53000
53200
J1600-3053 Time MJD 53118.6

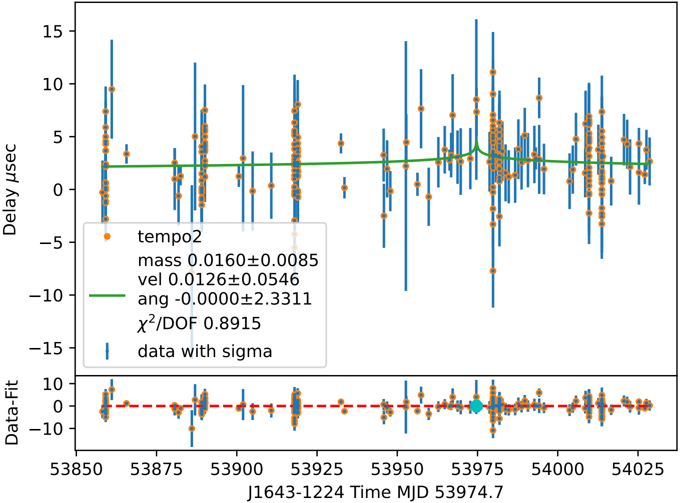

Delay μsec
15
10
5
0
−5
−10
−15
tempo2
mass 0.0160±0.0085
vel 0.0126±0.0546
ang -0.0000±2.3311
χ²/DOF 0.8915
data with sigma
Data-Fit
10
0
−10
53850
53875
53900
53925
53950
53975
54000
54025
J1643-1224 Time MJD 53974.7

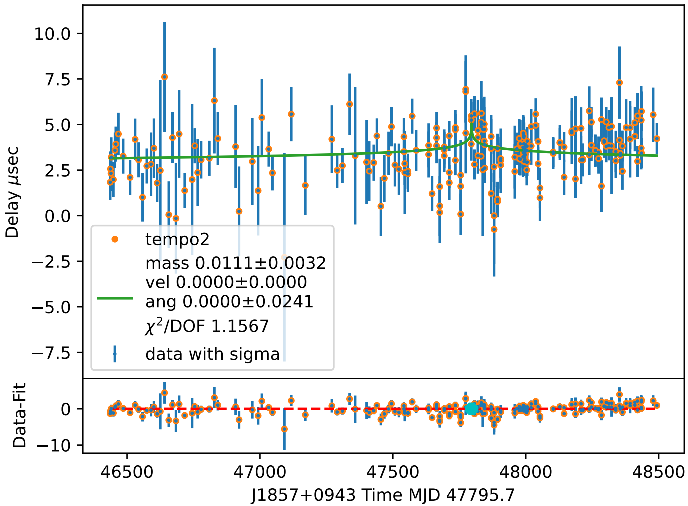
10.0
7.5
5.0
2.5
0.0
−2.5
−5.0
−7.5
Delay μsec
tempo2
mass 0.0111±0.0032
vel 0.0000±0.0000
ang 0.0000±0.0241
χ2/DOF 1.1567
data with sigma
Data-Fit
0
−10
46500
47000
47500
48000
48500
J1857+0943 Time MJD 47795.7